Changes in microtubule overlap length regulate kinesin-14-driven microtubule sliding

Marcus Braun[#,1,2,3], **Zdenek Lansky**[#,1,2,3], **Agata Szuba**[1,2], **Friedrich W. Schwarz**[1,2], **Aniruddha Mitra**[1,2], **Mengfei Gao**[1,2], **Annemarie Lüdecke**[1,2], **Pieter Rein ten Wolde**[4,*], and **Stefan Diez**[1,2,*]

[1]B CUBE - Center for Molecular Bioengineering, Technische Universität Dresden, Arnoldstraße 18, 01307 Dresden, Germany [2]Max Planck Institute of Molecular Cell Biology and Genetics, Pfotenhauerstraße 108, 01307 Dresden, Germany [3]Institute of Biotechnology CAS, BIOCEV, Prumyslova 595, Vestec 25250, Czech Republic [4]AMOLF, Science Park 104, 1098 XG Amsterdam, the Netherlands

[#] These authors contributed equally to this work.

Abstract

Microtubule-crosslinking motor proteins, which slide antiparallel microtubules, are required for remodeling of microtubule networks. Hitherto, all microtubule-crosslinking motors have been shown to slide microtubules at constant velocity until no overlap between the microtubules remains, leading to breakdown of the initial microtubule geometry. Here, we show *in vitro* that the sliding velocity of microtubules, driven by human kinesin-14, HSET, decreases when microtubules start to slide apart, resulting in the maintenance of finite-length microtubule overlaps. We quantitatively explain this feedback by the local interaction kinetics of HSET with overlapping microtubules, causing retention of HSET in shortening overlaps. Consequently, the increased HSET density in the overlaps leads to a density-dependent decrease in sliding velocity and the generation of an entropic force antagonizing the force exerted by the motors. Our results demonstrate that a spatial arrangement of microtubules can regulate the collective action of molecular motors through local alteration of their individual interaction kinetics.

Introduction

Molecular motors are enzymes that consume chemical energy to generate mechanical work. While their motor-domains step along cytoskeletal filaments, such as microtubules, their tail-domains interact with cargo proteins, or, in some cases, also interact with cytoskeletal filaments, thus establishing inter-filament crosslinks. Examples of microtubule crosslinking motors are members of the kinesin-14 family1, such as human HSET. HSET is known to slide short, nascent microtubules towards the spindle poles2 and, in concert with other microtubule sliding motors like kinesin-5 and dynein, HSET is involved in the focusing of the spindle poles3–6. In general, kinesin-14s are non-processive motor proteins, meaning that their motor-domains dissociate from the microtubule after a single step leading to sub-second dwell times7,8. Their tail-domains interact with microtubules diffusively over long timescales7–9. The collective action of kinesin-14 can lead to the sliding of overlapping antiparallel microtubules relative to each other8,10, resulting in large-scale rearrangements of cytoskeletal networks. At a given motor concentration, these motors have so far been observed to slide microtubules at constant velocity until no overlap between the microtubules remains8,9. In some cases, the microtubules can remain connected at their tips by a single point (presumably a single motor) leading to a pivoting motion of the microtubules8,11. Both possibilities lead to the disruption of the initially antiparallel geometry of the microtubule pair. To maintain the antiparallel microtubule geometry in the presence of continuous sliding by molecular motors, the regulation of molecular motor action is crucial. In particular, maintenance of antiparallel microtubule overlaps of finite length requires that molecular motors are prevented from sliding microtubules apart. Examples of such motor regulation, are to be found in the midzone of the mitotic spindles during cell division12 or in the interphase microtubule array of the fission yeast S. pombe13, where overlaps are maintained over tens of minutes12,14.

For this regulation, additional proteins are thought to be necessary. Examples are kinases and other protein-modifying enzymes, which conduct direct modifications of the molecular motors themselves (e.g. phosphorylation), or influence the motors indirectly by modifying other regulatory proteins15–19. Furthermore, motor action can be regulated by direct physical competition with other motors that generate force in the opposite direction. This regulation was shown to lead to directional instability of microtubule sliding, manifested by the sequential switching of sliding from one direction to the other9,20. Finally, molecular motors can be regulated by diffusible non-motor microtubule crosslinkers, such as the members of the Ase1/PRC1/Map65 family, which can act as adaptive brakes for motor-driven sliding21. For example, when microtubules are slid apart by the kinesin-14 Ncd, Ase1 crosslinkers remain in the shortening overlaps, generating entropic expansion forces that counteract the motors22. The presence of the crosslinkers can thus lead to the slowdown of motor-driven microtubule sliding, maintaining the antiparallel overlap geometry over tens of minutes21,23.

We here show that, without the need for additional regulatory proteins, regulation of molecular motors can result from the interplay between the spatial arrangement of microtubules and the kinetics of the molecular motors themselves. We found that HSET-driven microtubule sliding slows down with a decreasing length of the overlap between the

microtubules that are crosslinked by HSET. We quantitatively explain the regulatory feedback by rapid microtubule-(re)binding of the motor-domains of HSET molecules tethered by their tail-domains to the other microtubule in a microtubule overlap. As a consequence, HSET molecules are retained in the shortening overlap when microtubules start to slide apart, leading to an HSET density-dependent reduction of the sliding velocity through steric hindrance between the motors and an opposing entropic force generated by the overlap-bound motors. HSET molecules by themselves can thus maintain antiparallel overlaps between microtubules over tens of minutes demonstrating that partially overlapping microtubules can regulate the collective action of molecular motors.

Results

Change in overlap length affects HSET sliding velocity

To study the activity of HSET we generated green fluorescence protein (GFP)-tagged HSET (Supplementary results, Supplementary Fig. 1a, 1b and Methods), immobilized sparsely rhodamine-labeled 'template' microtubules on a coverslip and allowed GFP-HSET to interact with the microtubule lattice. When we added densely rhodamine-labeled 'transport' microtubules, we observed the formation of microtubule overlaps and, in the presence of ATP, directed microtubule sliding (Fig. 1, Methods). Consistent with previous results on *D. melanogaster* kinesin-14 Ncd8, we found that GFP-HSET crosslinks microtubules into both parallel and antiparallel geometries, but slides only antiparallel ones (Supplementary Fig. 1c). Similarly to *X. laevis* kinesin-14 XCTK29 but in contrast to GFP-Ncd21, we found that GFP-HSET preferentially interacted with overlapping microtubules (as compared to single microtubules), following the microtubule overlaps during microtubule sliding (Fig. 1b and 1c). We estimated the density of GFP-HSET in the overlaps as the integrated GFP intensity along the length of the overlaps divided by the overlap lengths (Methods). We found that, at 1.5 nM GFP-HSET in solution, the density of GFP-HSET in microtubule overlaps was approximately six times higher than on single microtubules.

Previous work on kinesin motors showed that transport microtubules continue to slide along template microtubules with constant velocity until no overlap between the microtubules remains8–11,24. By contrast, we found that HSET-driven motility of transport microtubules that initially moved with constant velocity, decelerated as the microtubules started to slide apart (Fig. 1b, 1c and Supplementary Movie 1). This slowdown resulted in the formation of microtubule overlaps with finite lengths, remaining in an antiparallel geometry for tens of minutes. This observation suggests that, unlike for other kinesin motors, the velocity of microtubule sliding driven by HSET is regulated in a manner that depends on the length of the microtubule overlap.

HSET sliding velocity depends on the motor density

We quantitatively analyzed the sliding velocities and the amount of GFP-HSET molecules in the shortening microtubule overlaps during events as presented in Fig. 1. We found that the total GFP-fluorescence intensity, reflecting the amount of GFP-HSET molecules in the shortening overlaps, remained approximately constant as the microtubules slid apart. This finding means that the density of GFP-HSET in shortening overlaps progressively increased,

suggesting that the ends of the microtubule overlaps constituted barriers that GFP-HSET molecules were not likely to cross (Fig. 2a and Supplementary Fig. 2a). Quantitative analysis of the efficiency of HSET confinement by the barriers revealed that upon halving the overlap length, about 84% of the initial amount of GFP-HSET remained in the overlap (Supplementary Fig. 2b, Methods). At the same time, the sliding velocity decreased with increasing HSET density in the microtubule overlaps (Fig. 2b).

To further explore the slowdown mechanism, we asked whether an increase in GFP-HSET density also reduces the sliding velocity of microtubules that are not sliding apart, but are overlapping over their full lengths, as observed before for XCTK29. Indeed, we found that the sliding velocity of transport microtubules fully overlapping with their template microtubules decreased with increasing GFP-HSET density ($n = 67$ microtubules; Fig. 2c). Intriguingly, we observed that for a given GFP-HSET density the fully overlapping microtubules were sliding on average faster than the microtubules sliding apart (repeated measures ANOVA, $p < 10^{-4}$; compare Fig. 2c and 2b). This finding suggests that not only the increase in density, but also the fact whether microtubules overlap fully or partially, plays a role in the slowdown.

Due to the high level of noise in the data presented in Fig. 2b and 2c, we aimed to assess the influence of the motor density on microtubule motility in an independent way. We coated glass coverslips with decreasing concentrations of GFP-HSET in solution, resulting in decreasing motors densities on the coverslip surfaces. When observing the gliding motility of microtubules on these surfaces (Methods), we found that a reduction in motor density resulted in a velocity increase (Fig. 2d). Because this increase was largely independent of the lengths of the gliding microtubules (Supplementary Fig. 2c), we reason that it is not the absolute number of motors, but rather their density (i.e. the spacing between the motors), which sets the gliding velocity.

To exclude the possibility that the N-terminal tail-domain of HSET, which in other kinesin-14 family members is known to interact with microtubules[8–10], influenced the observed motility, we created a truncated GFP-HSET construct lacking the tail-domain (for details on this construct see below, Supplementary Fig. 1a and Methods). We repeated our microtubule gliding experiments using this construct and obtained qualitatively identical results; the gliding velocity did depend on the surface density of HSET but not on the lengths of the gliding microtubules (Supplementary Fig. 2d). Taken together, these experiments demonstrate that at increased motor density, HSET propels microtubules at decreased velocities.

HSET diffuses in microtubule overlaps

To assess the molecular mechanism of HSET confinement to microtubule overlaps, we characterized the interaction of individual GFP-HSET molecules with single and overlapping microtubules in the presence of ATP. We formed microtubule overlaps similarly to the experiment presented in Fig. 1, using a low concentration (0.15 nM) of unlabeled HSET. After addition of GFP-HSET we observed the diffusible interaction of GFP-HSET molecules with single microtubules (diffusion constant of $0.39 \pm 0.01\ \mu m^2\ s^{-1}$, $n = 22$ events, mean $\pm$ SEM) and overlapping microtubules (diffusion constant of 0.021 ± 0.005

$\mu m^2\ s^{-1}$, $n = 14$ events, Fig. 3a, Supplementary Fig. 3a and 3b). We attribute this drastic reduction of the diffusion constant to the simultaneous interaction of GFP-HSET molecules with both overlapping microtubules (see also numerical simulations below). To address the question if the ATPase activity of the motor is required to reduce the diffusion constant of GFP-HSET in microtubule overlaps we exchanged the ATP-containing buffer for a buffer containing ADP. Under these conditions, the observed diffusion was similar to the diffusion in the presence of ATP, both on single microtubules and in microtubule overlaps (Fig. 3b), indicating that the nucleotide state of the motor-domain had no influence on GFP-HSET diffusibility. In both cases, we frequently observed individual GFP-HSET molecules switching from fast to slow diffusion when they moved from a single microtubule into a microtubule overlap (Fig. 3a, events marked by red arrow). On rare occasion, we observed single GFP-HSET molecules moving out of a microtubule overlap, switching from slow to fast diffusion (Fig. 3a, event marked by black arrow). The episodic nature of the latter events indicates, that this kind of transition was possible, but energetically unfavorable. In combination, these experiments exemplify on the single molecule level, the presence of diffusion barriers at the ends of microtubule overlaps as discussed above (Fig. 2a, Supplementary Fig. 2a and 2b). These barriers effectively confine the movement of GFP-HSET to microtubule overlaps. Importantly, diffusion in microtubule overlaps allows GFP-HSET to follow the overlap when the microtubules are sliding.

We hypothesized that, analogously to other kinesin-14 motors[8,10,25], the specific interactions of GFP-HSET with microtubules depended on two microtubule-interaction domains at the opposing ends of the primary amino-acid sequence. We therefore aimed at dissecting the relative contributions of these two interaction domains on the diffusion of GFP-HSET, both on single microtubules and in microtubule overlaps. Based on computational structural predictions and information available from other kinesin-14 family members[25–27], we generated two truncated homodimeric GFP-HSET constructs consisting of the coiled-coil with either only the HSET motor-domain (GFP-HSET-motor) or only the HSET tail-domain (GFP-HSET-tail) (Fig. 3c, Supplementary Fig. 1a and Methods). Using either truncated construct, microtubule overlaps failed to form (though we varied the HSET concentrations up to 75 nM), indicating that motor- and tail-domains are required simultaneously to form a crosslink between two microtubules. When preforming microtubule overlaps by 0.15 nM unlabeled full-length HSET we found that on single microtubules GFP-HSET-tail exhibited a diffusion constant of $0.41 \pm 0.02\ \mu m^2\ s^{-1}$ ($n = 22$ events, mean ± SEM) and a dwell time on the order of minutes (Fig. 3d and Supplementary Fig. 3c). Both values were not significantly different from the values obtained with full-length GFP-HSET, suggesting that HSET interacts with a single microtubule predominantly via its tail-domain, consistent with previous work on *D. melanogaster* kinesin-14[8]. Within microtubule overlaps, we observed that GFP-HSET-tail diffused in a similar manner as on single microtubules, however, interestingly freely moving across the overlap ends (Fig. 3d; events marked by arrows). GFP-HSET-motor exhibited only short interactions with individual microtubules and overlapping microtubules, with a rate of unbinding of 4.1 ± 0.9 s^{-1} (95 % confidence interval, $n = 473$ events, Fig. 3e and Supplementary Fig. 3d). In fact, the dwell time of GFP-HSET-motor was too short to detect any movement of the molecules along the microtubules.

In contrast to the full length HSET, whose diffusion slowed down in the overlaps, the truncated constructs interacted with single microtubules and overlapping microtubules in the same manner. As the diffusion constant of the tail was the same as the diffusion constant of the full-length HSET on single microtubules, we argue that it is the additional interaction of the motor-domain of full-length HSET with an adjacent microtubule that lowers the diffusion constant of full length HSET in the overlap.

HSET generates entropic forces in partial overlaps

For given GFP-HSET densities, the sliding velocities of partially-overlapping microtubules were lower than for fully overlapping microtubules (Fig. 2b and 2c), showing that the density-dependence of HSET-driven microtubule sliding alone cannot quantitatively explain the slowdown of sliding observed in Fig. 1. Our single-molecule experiments revealed that GFP-HSET diffusion was confined by the ends of the microtubule overlaps acting as diffusion barriers. We thus asked whether, analogously to previous work where confined, diffusible microtubule crosslinkers generated entropic forces promoting an increase in overlap length[22], HSET was able to counteract its motor-domain-generated forces by a similar mechanism. To address this question, we decoupled the ATP-dependent motor-domain-generated force from the putative ATP-independent entropic force by forming microtubule overlaps in the presence of 1 mM ADP (0 mM ATP, Fig. 4). In this scenario GFP-HSET crosslinked microtubules, but did not induce directional sliding (zero sliding events from the total of $n = 36$ observed fully overlapping microtubule pairs). To move the transport microtubules relative to the template microtubules, we applied a hydrodynamic flow to the motility buffer. Partial microtubule overlaps were created when the transport microtubules started sliding over the ends of their template microtubules. After stopping the hydrodynamic flow, we observed that the transport microtubules started moving backwards in the direction of increasing overlap lengths (Fig. 4a-c). We observed neither movement of partially overlapping microtubules in the direction of decreasing overlap length nor did we observe any directional movement of transport microtubules that fully overlapped with their template microtubules. We estimated the amount of HSET molecules in the microtubule overlaps during overlap expansion and found that it was approximately constant (Supplementary Fig. 4). Thus, no additional HSET molecules from solution bound into the microtubule overlaps, indicating that overlap expansion was not driven by changes in enthalpy[22]. Analyzing the sliding velocities, we found that they were inversely proportional to the length of the overlap (Fig. 4d). Taken together, these findings suggest that HSET molecules confined in partial microtubule overlaps generate entropic forces (similar to microtubule crosslinkers of the PRC1/Ase1/MAP65 family[22]), acting analogously to confined gas particles generating a pressure. Consequently, when HSET slides microtubules apart, the motors have to work against an increasing entropic force as the overlap length decreases.

Binding kinetics explain HSET diffusion in the overlaps

We numerically modeled the slowdown of HSET-driven microtubule sliding based on our experimental findings. We simulated the HSET molecules as harmonic springs, whose ends hop randomly (tail-domain) and directionally (motor-domain) along two one-dimensional arrays of binding sites representing the microtubules (Fig. 5a, Methods). The hopping and

unbinding rates of the two interaction sites were determined from the experimentally measured diffusion constant, motor velocity and dwell times (Methods). Because, on a single microtubule the tail-domain has a much longer dwell time than the motor-domain, most HSET molecules are tethered to a microtubule via their tail-domains at any given time. When located in a microtubule overlap, a tethered HSET molecule can thus easily bind to the adjacent microtubule via its motor-domain. In this geometry, the time for the motor-domain to find a microtubule binding-site will be much shorter than that for the motor-domain of an HSET molecule freely diffusing in solution. Tethering thus effectively raises the net binding rate of the motor-domain, which is reflected in the simulation by two different motor-domain binding rates: (i) $k_{on}^{motor(solution)}$ describing the binding rate from solution (set to match the experimentally observed densities of HSET molecules on single microtubules) and (ii) $k_{on}^{motor(tethered)}$ describing the binding rate of the motor domain of a tethered HSET molecule. With regard to the latter, we observed that the diffusion constant of HSET in the overlap decreased as $k_{on}^{motor(tethered)}$ was increased, indicating that diffusion slows down when HSET is more often bound to both microtubules. We found that the experimentally observed diffusion constant was reproduced for $k_{on}^{motor(tethered)} = 60$ s^{-1} (Fig. 5b, see Methods for further details). This value indicates, that after detachment, the motor-domain will rebind rapidly (1/ $k_{on}^{motor(tethered)} \sim 0.02$ s) to the microtubule. During this time, the HSET molecule can move by its tail-mediated diffusion only a short distance, suggesting that HSET molecules, at the ends of the microtubule overlaps are likely to rebind by their motor-domains to the overlap and are therefore unlikely to leave the overlap. Our simulations thus explain how the binding kinetics of HSET together with the spatial arrangement of the microtubules lead to the experimentally observed slow diffusion of HSET inside microtubule overlaps and to the confinement of HSET within microtubule overlaps.

Confinement explains HSET sliding velocity regulation

We hypothesize that the slowdown of microtubules that slide apart (Fig. 1 and 2) can be explained by the confinement of HSET to the microtubule overlap. To test this hypothesis we performed simulations, keeping all the parameters as determined above for single HSET molecules. We first simulated the sliding of a transport microtubule that fully overlaps with a template microtubule. We varied the density of HSET molecules in the microtubule overlap (by changing the length of the transport microtubule while keeping the total number of HSET molecules inside the overlap constant). Similarly to our experiments (Fig. 2c), we observed that the sliding velocity decreased with increasing motor density (Fig. 5c).

Next we simulated the experiments in which two microtubules are connected by HSET molecules, forming a partial overlap in the presence of ADP (in the absence of ATP). We simulated this condition by setting the force that a motor can generate to zero. As in the experiments (Fig. 4), we observed that the filaments moved in the direction of increasing overlap length and that the velocity of sliding was inversely proportional to the length of the overlap (Fig. 5d and 5e). This effect is due to the entropic expansion force that is generated by the HSET molecules confined inside the microtubule overlap.

Finally, we simulated the situation where transport and template microtubules slide apart in the presence of ATP (Fig. 6a, 6b, 6c and Supplementary Fig. 5b). Similarly to the experiment presented in Fig. 1, we observed that, as the microtubules started to slide apart and the microtubule overlap shortened, HSET molecules became compacted in the overlap (about 88% of the initial HSET molecules were retained in the overlap when the overlap length was halved) leading to an increase in the HSET density (Fig. 6a, 6b and Supplementary Fig. 5a). With increasing HSET density the velocity of sliding decreased (Fig. 6c) resulting in the maintenance of an antiparallel microtubule overlap of finite length for tens of minutes (Fig. 6a). When, in our simulations, we either i) reduced the binding rate of the tethered motor domain $k_{on}^{motor(tethered)}$, or ii) increased the unbinding rate of the tail-domain k_{off}^{tail}, we found that HSET was not retained in the overlap and that the microtubules separated (Supplementary Fig. 5c and 5d). This finding predicts that the binding kinetics of the overlap-bound HSET molecules critically contributes to whether the diffusible motors will be confined by the barriers at the ends of the overlap. To test this prediction we repeated our experiments in buffer with increased ionic strength (Methods), expected to reduce the strength of electrostatic interactions. Indeed, on the single molecule level, we observed a drastic reduction of the dwell time of the HSET tail on single microtubules (Supplementary Fig. 6a). When we repeated the experiment from Fig. 1 at these conditions, we observed that HSET was not retained in the shortening overlaps anymore and that the microtubules slid apart at constant velocity until they separated (Supplementary Fig. 6b and 6c). These results confirm the predictions of our model.

Moreover, our simulations reproduce the experimental observation (Fig. 2b and 2c) that for a given HSET concentration the sliding velocity is on average higher for transport microtubules that fully overlap with their template microtubules as compared to transport microtubules that slide apart and thus overlap with the template microtubules only partly (repeated measures ANOVA, $p < 10^{-4}$; compare Fig. 5c and 6c). This difference is due to the entropic force, which can manifest itself only when the length of the microtubule overlap changes, which is the case only when the microtubules overlap partly. Our simulations thus enable us to differentiate between the two effects that lead to the decrease in sliding velocity when microtubules slide apart, namely i) the HSET-density dependence of the sliding velocity and ii) the entropic force acting against the force generated by the motor-domain. Together, our experimental and theoretical results reveal a feedback mechanism, which drastically slows down HSET-driven sliding of partially overlapping microtubules and prevents microtubule separation (Fig. 6d, 6e).

Discussion

HSET-driven microtubule sliding decelerates when the microtubules start to slide apart due to a feedback mechanism that regulates the sliding in two ways. (1) The sliding velocity decreases with increasing HSET density. This effect, similar to concentration-dependent sliding velocities observed for XCTK29, can be explained by either a decrease in the collective motor force driving the sliding or an increase in the friction between the overlapping microtubules. We hypothesize that these effects might be due to steric hindrance between the motors (in particular between the motor domains, as the motor-density dependent slow down is also observed in the gliding geometry with tail-less HSET), which

might result in lowering the average stepping rate. In our simulations, we indeed observe individual molecules in the overlap frequently coming into contact with each other. Experimentally, likewise, mean square displacement analysis of the motion of single GFP-HSET molecules in the overlap suggests that HSET molecules cannot pass each other in the microtubule overlap and thus hinder each other's motion (Supplementary Fig. 3b). Interestingly, steric blocking was recently also reported to regulate the motility of kinesin-5 by reversing the stepping direction[28]. (2) The sliding velocity is regulated through an entropic force generated by the HSET molecules confined in the overlap. HSET entropic force generation provides a new example of a general mechanism of entropic expansion of confined diffusible crosslinkers described earlier[22]. Diffusibility of the crosslinkers in the overlap is a prerequisite for this mechanism. Although HSET does not have two diffusible microtubule-binding sites, nevertheless, due to its motor-domain exhibiting a high rate of binding and unbinding from the microtubule, HSET molecules effectively act as diffusible crosslinkers in the overlap.

We show that a low turnover of HSET between microtubule overlaps and solution is essential for the regulation of HSET. HSET binds to microtubules predominantly with its tail-domain, scanning the surface of this microtubule via diffusion. When it encounters a second, adjacent, microtubule during this process, it swiftly interacts with it via its motor-domain. Once the motor-domain unbinds from the second microtubule, it remains positioned close to the surface of this microtubule due to tail-domain tethering on the other microtubule, leading to a rapid rebinding of the motor-domain. The tail-domain tethering of HSET molecules to a microtubule thus enables HSET to maintain the crosslink between two microtubules despite being a non-processive motor with rather high unbinding rates of its motor-domain from isolated microtubules (Fig. 6a). The net binding rate at which a motor-domain will bind is given by the association rate constant times the local concentration. Tethering can thus be understood as raising the effective local concentration of the motor-domains inside the overlap, above the concentration in solution. Similarly, tethering by one binding site to the microtubule lattice enables processivity of the heterodimeric kinesin-14 Cik1-Kar3[29]. Tail-domain tethering was also shown to act as a switch in the directionality of kinesin-14 KlpA[30] and a similar mechanism might be also responsible for the directionality switch in homo-tetrameric kinesin-5[31].

Regulation of HSET is based on the increase in the HSET density in overlaps when microtubules slide apart due to the low probability of HSET unbinding from the overlap. We explain this low probability by the interplay between the binding kinetics and the diffusion of HSET along the microtubule lattice. When the motor-domain unbinds, the HSET molecule can diffuse only a short distance along the surface of the microtubule by its tail-domain before the motor-domain rebinds. Given the length and flexibility of the HSET molecule, it is very likely to rebind back to the overlap. The overlap ends thus effectively act as diffusion barriers for HSET. We show that the efficiency of retaining HSET molecules by this barrier can be tuned by the HSET binding kinetics. We hypothesize that *in vivo* the binding kinetics, and thus the efficiency of retention, can be tuned by binding of additional proteins or posttranslational modifications of the microtubule binding sites of HSET or of the microtubule lattice. For example, kinesin-14s are known to have multiple

phosphorylation sites[32], and it has been shown that phosphorylation can alter the interaction of other kinesin-14[18] and also kinesin-5[17,33] motors with microtubules.

How do other kinesin-14 motors interact with microtubule overlaps? For the *D. melanogaster* Ncd no preferential localization in the overlap was observed[8], demonstrating that the overlap ends do not constitute barriers for Ncd[21]. On the other hand, *X. laevis* kinesin-14, XCTK2 has been shown to preferentially locate to microtubule overlaps and to slide microtubules at lower velocities when the motor concentration is increased. Notably, however, no slowdown of XCTK2-induced motility has been observed for microtubules sliding apart. We explain this by the fact that the density of XCTK2 does not increase in the shortening overlaps when the microtubules slide apart. As the tail-domain diffusion constant of XCTK2 ($D_{XCTK2} = 0.1 \ \mu m^2/s$) is almost identical to that of HSET, the difference in the collective action of both motors might be explained by the shorter microtubule dwell time of the XCTK2 tail-domain of about 3 s (ref. 9) and/or a slower rebinding rate of the tethered XCTK2 motor-domain, leading to a faster turnover of XCTK2 molecules in microtubule overlaps. A rapid exchange between overlap and solution can also explain why XCTK2 molecules seem to apparently follow moving overlaps[9]: individual molecules are likely not retained in the overlap, but continuously shuttle between overlap and solution. As the turnover kinetics might depend on the posttranslational modification of either the tail-domain or the motor-domain, we speculate that also other kinesin-14s, such as XCTK2 or Ncd, could potentially undergo modifications decreasing their turnover in the overlap and enabling a regulatory feedback mechanism analogous to HSET.

Methods

Protein purification

Full-length N-terminal hexa-histidine tagged HSET (1-673 aa) and GFP-HSET (1-673 aa) were expressed in Drosophila SF9 insect cells using a Bac-to-Bac Expression System (Invitrogen). N-terminal hexa-histidine tagged GFP-HSET-tail (1-315 aa) and GFP-HSET-motor (145-673aa) were expressed in insect cells using flashBAC System (Oxford Expression Technologies). Harvested cells were resuspended in purification buffer (50 mM sodium phosphate buffer pH 7.5, 1 mM MgCl$_2$, 10 mM 2-mercaptoethanol, 300 mM NaCl, 0.1% Tween20 w/vol, 10% glycerol w/vol, 30 mM imidazole and EDTA-free protease inhibitors (Roche)). Crude lysate was centrifuged at 20,000g at 4°C and loaded on NiNTA resin (Qiagen). The resin was washed with purification buffer containing 60 mM imidazole. Proteins were eluted in purification buffer containing 300 mM imidazole, snap-frozen in liquid nitrogen and stored at -80°C. Size and purity of all constructs was checked by SDS-PAGE gel. Analytical size exclusion chromatography using Sepharose 6 (GE Healthcare) in 20 mM HEPES pH 7.2, 1 mM EGTA, 75 mM KCl, 2 mM MgCl$_2$, 0.1 mM ATP (+Mg), 10 mM dithiothreitol and 0.1% Tween confirmed that the proteins were monodisperse. For control motility experiments, insect-cell expressed GFP-HSET was first bound to the NiNTA resin in purification buffer and then cleaved off the resin using His-tagged TEV protease.

In vitro motility assays

(i) *For microtubule sliding experiments*, template microtubules, transport microtubules and flow cells were prepared as described previously8. First, biotinylated, paclitaxel-stabilized, sparsely rhodamine-labeled template microtubules in BRB80 (80 mM Pipes/KOH pH 6.9, 1 mM MgCl$_2$, 1 mM EGTA) were immobilized in a flow chamber using biotin antibodies (Sigma B3640, 40 μg ml^{-1} in PBS). Secondly, the buffer in the flow cell was exchanged for assay buffer (20 mM HEPES pH7.2, 1 mM EGTA, 75 mM KCl, 2 mM MgCl$_2$, 1 mM ATP (+Mg), 10 mM dithiothreitol, 0.5mg/ml casein, 10 μM paclitaxel, 0.1% Tween, 10% w/v sucrose, 20 mM d-glucose, 110 μg/ml glucose oxidase and 20 μg/ml catalase). Thirdly, the respective HSET construct in assay buffer was flushed into the flow cell at final assay concentrations. Fourthly, densely rhodamine-labeled, non-biotinylated transport microtubules in assay buffer were flushed into the flow cell and were allowed to bind to the template microtubules via HSET. Finally, the chamber was rinsed with assay buffer containing the HSET construct at the final assay concentration. This last step removed unbound transport microtubules from solution. For experiments showing HSET-dependent overlap expansion, the buffer flush in the final step did not contain any HSET molecules. For experiments at increased ionic strength, the buffer flush in the final step contained additional 75 mM, 100 mM, 125 mM or 150 mM KCl. To verify that the hexa-histidine tag used for the affinity purification of the GFP-HSET construct did not affect the interaction of the protein with microtubules, we performed a set of control experiments using the construct with the hexa-histidine tag cleaved off, showing qualitatively identical results to those presented in Fig. 1 (Supplementary Fig. 1d). All experiments were performed at 24°C. (ii) *For microtubule gliding experiments with full-length HSET*, detergent-cleaned coverslips were used to prepare the flow cells. First, casein buffer (20 mM HEPES pH 7.2, 1 mM EGTA, 75 mM KCl, 2 mM MgCl$_2$, 0.5 mg/ml casein) was flushed into the flow cell. Secondly, the HSET molecules in assay buffer were flushed into the flow cell. Thirdly, densely rhodamine-labeled microtubules were flushed in and allowed to bind to the HSET molecules. Finally, the chamber was rinsed with assay buffer to remove unbound microtubules. (iii) *For microtubule gliding experiments with the GFP-HSET-motor*, dichlorodimethylsilane (DDS)-silanized coverslips were used to prepare the flow cells. First, GFP-HSET-motor constructs were immobilized in the flow chamber using anti-GFP monoclonal antibodies (mouse, MPI-CBG antibody facility). The surface density of GFP-HSET-motor was set by the concentration of the antibodies used to coat the coverslip surface. Secondly, densely rhodamine-labeled microtubules were flushed in and finally the chamber was rinsed with assay buffer.

Imaging

(i) *In microtubule gliding experiments*, rhodamine-labeled microtubules were visualized with an acquisition rate of 1 frame per second in the TRITC channel. (ii) *In microtubule sliding experiments*, rhodamine-labeled microtubules and GFP-labeled HSET motors were visualized sequentially by switching between TRITC and GFP channels using a setup described previously34 with acquisition rates of 1 frame per 5 seconds for the TRITC channel and 1 frame per 25 seconds for the GFP channel. To visualize the interaction of single GFP-labeled molecules with microtubules, the GFP-channel acquisition rate was 1 frame per 100 milliseconds. Experiments were performed over several months. *N* = 33

events of two microtubules sliding apart were observed during eight independent experimental days. Only microtubule pairs (single transport microtubules sliding along single template microtubules) were analyzed. From these events, none were excluded. $N =$ 67 events of transport microtubules sliding with their full lengths on template microtubules were chosen randomly from the same videos.

Image analysis

Microtubule sliding experiments were analyzed by custom written Matlab (Mathworks) routines. The position of the transport microtubule relative to the template microtubule was measured in each frame. The sliding velocity was calculated from positional data of the transport microtubules using a rolling frame average over nine frames. When template and transport microtubules were fully overlapping, the location of the overlap was identified as the location of the transport microtubule. When the microtubules were sliding apart, the location of the shortening overlap was estimated from the position of the trailing (minus) end of the transport microtubule and the position of the minus end of the template microtubule. The location of the overlap was used in every frame to estimate the overlap length and as a mask to read out the total amount of overlap-bound GFP-HSET. The GFP-HSET signal in regions directly adjacent to the mask was subtracted as background signal. The efficiency of the GFP-HSET retention in the shortening overlaps and the fluorescent signal of a single GFP-HSET molecule was determined as described previously[21]. The density of GFP-HSET in microtubule overlaps was estimated as the number of HSET molecules per unit length in the overlap. Single-molecule diffusion traces were tracked using FIESTA software[35] and the diffusion constants were calculated from the mean-square-displacement values.

Mathematical modeling

HSET molecules were modeled as harmonic springs with two distinct microtubule-binding sites (motor-domain and tail-domain) at opposite ends of the spring. Microtubules were modeled as one-dimensional arrays of binding sites for HSET tail and motor domains. When interacting with microtubules, HSET molecules mutually excluded each other and could not pass each other, as suggested by experimental evidence (Supplementary Fig. 3b).

HSET was modeled to bind from solution to a single microtubule with one of its binding sites with the rates $k_{on}^{motor(solution)}$ and $k_{on}^{tail(solution)}$. When HSET was already bound with one of its binding sites to a single microtubule, it could dissociate from it into solution with rates $k_{off}^{motor(solution)}$ and $k_{off}^{tail(solution)}$. An HSET molecule, which was tethered to one of the microtubules by one of its binding sites, could associate with the second microtubule by its second binding site with rates $k_{on}^{motor(tethered)}$ and $k_{on}^{tail(tethered)}$. An HSET molecule, which was bound by both of its binding sites to two microtubules, could dissociate from one of the microtubules by one of its binding sites with rates $k_{off}^{motor(tethered)}$ and $k_{off}^{tail(tethered)}$. The rates of (un)binding of a tethered HSET molecule were dependent on the tension of the spring as described in[22]. When bound to the microtubule, the tail-domain could hop with equal probability $k_+ = k_-$, to the two neighboring (vacant) binding sites and was modeled as described earlier[22]. For the motor-domain, the hopping probabilities, k_+ and k_-, were asymmetric. The net speed of a single molecular motor was then $v = \delta (k_+ - k_-)$, where δ is

the spacing of the lattice. The maximum stall force of the molecular motor $F_{\max}$ was characterized as $k_+ / k_- = \exp[-F_{\max}\,\delta / k_B T]$, where k_B is the Boltzmann constant and T is the absolute temperature.

The parameters used for the simulations are summarized in Supplementary Table 1. We assumed that, in absence of tension on the spring, the values of the tethered tail- and motor-domain unbinding rates $k_{\mathrm{off}}^{\mathrm{tail(tethered)}}$ and $k_{\mathrm{off}}^{\mathrm{motor(tethered)}}$ would be equal to the values of their unbinding rates to solution $k_{\mathrm{off}}^{\mathrm{tail(solution)}}$ and $k_{\mathrm{off}}^{\mathrm{motor(solution)}}$, respectively. The experimentally determined dwell time of the tail-domain on a microtubule was orders of magnitude longer than the dwell time of the motor-domain, suggesting that the interaction of a full-length motor with a microtubule would be predominantly tail-mediated. The effective diffusion constant of an HSET molecule in an overlap (i.e. bound between two microtubules) thus depended on the tail-domain and the motor-domain hopping rates as well as on the attachment and the detachment rates of the motor-domain of a tail-tethered motor $k_{\mathrm{on}}^{\mathrm{motor(tethered)}}$ and $k_{\mathrm{off}}^{\mathrm{motor(tethered)}}$. We exploited the dependence on $k_{\mathrm{on}}^{\mathrm{motor(tethered)}}$ to match the experimentally-measured diffusion constant of HSET in an overlap. $k_{\mathrm{on}}^{\mathrm{motor(solution)}}$ and $k_{\mathrm{on}}^{\mathrm{tail(solution)}}$ were set to match the experimentally observed densities of HSET molecules on single microtubules. The algorithm used to simulate the model is described in22.

Supplementary Material

Refer to Web version on PubMed Central for supplementary material.

Acknowledgements

References

1. She Z-Y, Yang W-X. Molecular mechanisms of kinesin-14 motors in spindle assembly and chromosome segregation. J Cell Sci. 2017; 130:2097–2110. [PubMed: 28668932]

2. Cai S, Weaver LN, Ems-McClung SC, Walczak CE. Kinesin-14 Family Proteins HSET/XCTK2 Control Spindle Length by Cross-Linking and Sliding Microtubules. Mol Biol Cell. 2009; 20:1348–1359. [PubMed: 19116309]

3. Goshima G, Nédélec F, Vale RD. Mechanisms for focusing mitotic spindle poles by minus end-directed motor proteins. J Cell Biol. 2005; 171:229–240. [PubMed: 16247025]

4. Lecland N, Lüders J. The dynamics of microtubule minus ends in the human mitotic spindle. Nat Cell Biol. 2014; 16:770–778. [PubMed: 24976384]

5. Kwon M, et al. Mechanisms to suppress multipolar divisions in cancer cells with extra centrosomes. Genes Dev. 2008; 22:2189–2203. [PubMed: 18662975]

6. Watts CA, et al. Design, synthesis, and biological evaluation of an allosteric inhibitor of HSET that targets cancer cells with supernumerary centrosomes. Chem Biol. 2013; 20:1399–1410. [PubMed: 24210220]

7. deCastro M, Fondecave R, Clarke L, Schmidt CF, Stewart R. Working strokes by single molecules of the kinesin-related microtubule motor ncd. Nat Cell Biol. 2000; 2:724–729. [PubMed: 11025663]

8. Fink G, et al. The mitotic kinesin-14 Ncd drives directional microtubule-microtubule sliding. Nat Cell Biol. 2009; 11:717–723. [PubMed: 19430467]

9. Hentrich C, Surrey T. Microtubule organization by the antagonistic mitotic motors kinesin-5 and kinesin-14. J Cell Biol. 2010; 189:465–480. [PubMed: 20439998]

10. Braun M, Drummond DR, Cross RA, McAinsh AD. The kinesin-14 Klp2 organizes microtubules into parallel bundles by an ATP-dependent sorting mechanism. Nat Cell Biol. 2009; 11:724–730. [PubMed: 19430466]

11. Kapitein LC, et al. The bipolar mitotic kinesin Eg5 moves on both microtubules that it crosslinks. Nature. 2005; 435:114–118. [PubMed: 15875026]

12. Yamashita A. The Roles of Fission Yeast Ase1 in Mitotic Cell Division, Meiotic Nuclear Oscillation, and Cytokinesis Checkpoint Signaling. Mol Biol Cell. 2005; 16:1378–1395. [PubMed: 15647375]

13. Janson ME, et al. Crosslinkers and motors organize dynamic microtubules to form stable bipolar arrays in fission yeast. Cell. 2007; 128:357–368. [PubMed: 17254972]

14. Schuyler SC, Liu JY, Pellman D. The molecular function of Ase1p: evidence for a MAP-dependent midzone-specific spindle matrix. Microtubule-associated proteins. J Cell Biol. 2003; 160:517–528. [PubMed: 12591913]

15. Khmelinskii A, Roostalu J, Roque H, Antony C, Schiebel E. Phosphorylation-dependent protein interactions at the spindle midzone mediate cell cycle regulation of spindle elongation. Dev Cell. 2009; 17:244–256. [PubMed: 19686685]

16. Fu C, et al. Phospho-regulated interaction between kinesin-6 Klp9p and microtubule bundler Ase1p promotes spindle elongation. Dev Cell. 2009; 17:257–267. [PubMed: 19686686]

17. Cahu J, et al. Phosphorylation by Cdk1 increases the binding of Eg5 to microtubules in vitro and in Xenopus egg extract spindles. PLoS ONE. 2008; 3:e3936. [PubMed: 19079595]

18. Mana-Capelli S, McLean JR, Chen C-T, Gould KL, McCollum D. The kinesin-14 Klp2 is negatively regulated by the SIN for proper spindle elongation and telophase nuclear positioning. Mol Biol Cell. 2012; 23:4592–4600. [PubMed: 23087209]

19. Andrews PD, et al. Aurora B regulates MCAK at the mitotic centromere. Dev Cell. 2004; 6:253–268. [PubMed: 14960279]

20. Tao L, et al. A Homotetrameric Kinesin-5, KLP61F, Bundles Microtubules and Antagonizes Ncd in Motility Assays. Curr Biol. 2006; 16:2293–2302. [PubMed: 17141610]

21. Braun M, et al. Adaptive braking by Ase1 prevents overlapping microtubules from sliding completely apart. Nat Cell Biol. 2011; 13:1259–1264. [PubMed: 21892183]

22. Lansky Z, et al. Diffusible crosslinkers generate directed forces in microtubule networks. Cell. 2015; 160:1159–1168. [PubMed: 25748652]

23. Johann D, Goswami D, Kruse K. Generation of Stable Overlaps between Antiparallel Filaments. Phys Rev Lett. 2015; 115:118103. [PubMed: 26406858]

24. Sturgill EG, et al. Kinesin-12 Kif15 targets kinetochore fibers through an intrinsic two-step mechanism. Curr Biol. 2014; 24:2307–2313. [PubMed: 25264249]

25. Chandra R, Salmon ED, Erickson HP, Lockhart A, Endow SA. Structural and functional domains of the Drosophila ncd microtubule motor protein. J Biol Chem. 1993; 268:9005–9013. [PubMed: 8473343]

26. Lupas A, Van Dyke M, Stock J. Predicting coiled coils from protein sequences. Science. 1991; 252:1162–1164. [PubMed: 2031185]

27. Karabay A, Walker R. Identification of microtubule binding sites in the Ncd tail domain. Biochemistry. 1999; 38:1838–1849. [PubMed: 10026264]

28. Britto M, et al. Schizosaccharomyces pombe kinesin-5 switches direction using a steric blocking mechanism. Proceedings of the National Academy of Sciences. 2016; 113:E7483–E7489.

29. Mieck C, et al. Non-catalytic motor domains enable processive movement and functional diversification of the kinesin-14 Kar3. Elife. 2015; 4

30. Popchock AR, et al. The mitotic kinesin-14 KlpA contains a context-dependent directionality switch. Nat Commun. 2017; 8:13999. [PubMed: 28051135]

31. Düselder A, et al. Deletion of the Tail Domain of the Kinesin-5 Cin8 Affects Its Directionality. Journal of Biological Chemistry. 2015; 290:16841–16850. [PubMed: 25991727]

32. Molodtsov MI, et al. A Force-Induced Directional Switch of a Molecular Motor Enables Parallel Microtubule Bundle Formation. Cell. 2016; 167:539–552.e14. [PubMed: 27716509]

33. Shapira O, Gheber L. Motile properties of the bi-directional kinesin-5 Cin8 are affected by phosphorylation in its motor domain. Sci Rep. 2016; 6:25597. [PubMed: 27216310]

34. Braun M, et al. The human kinesin-14 HSET tracks the tips of growing microtubules in vitro. Cytoskeleton (Hoboken, NJ). 2013; 70:515–521.

35. Ruhnow F, Zwicker D, Diez S. Tracking Single Particles and Elongated Filaments with Nanometer Precision. Biophys J. 2011; 100:2820–2828. [PubMed: 21641328]
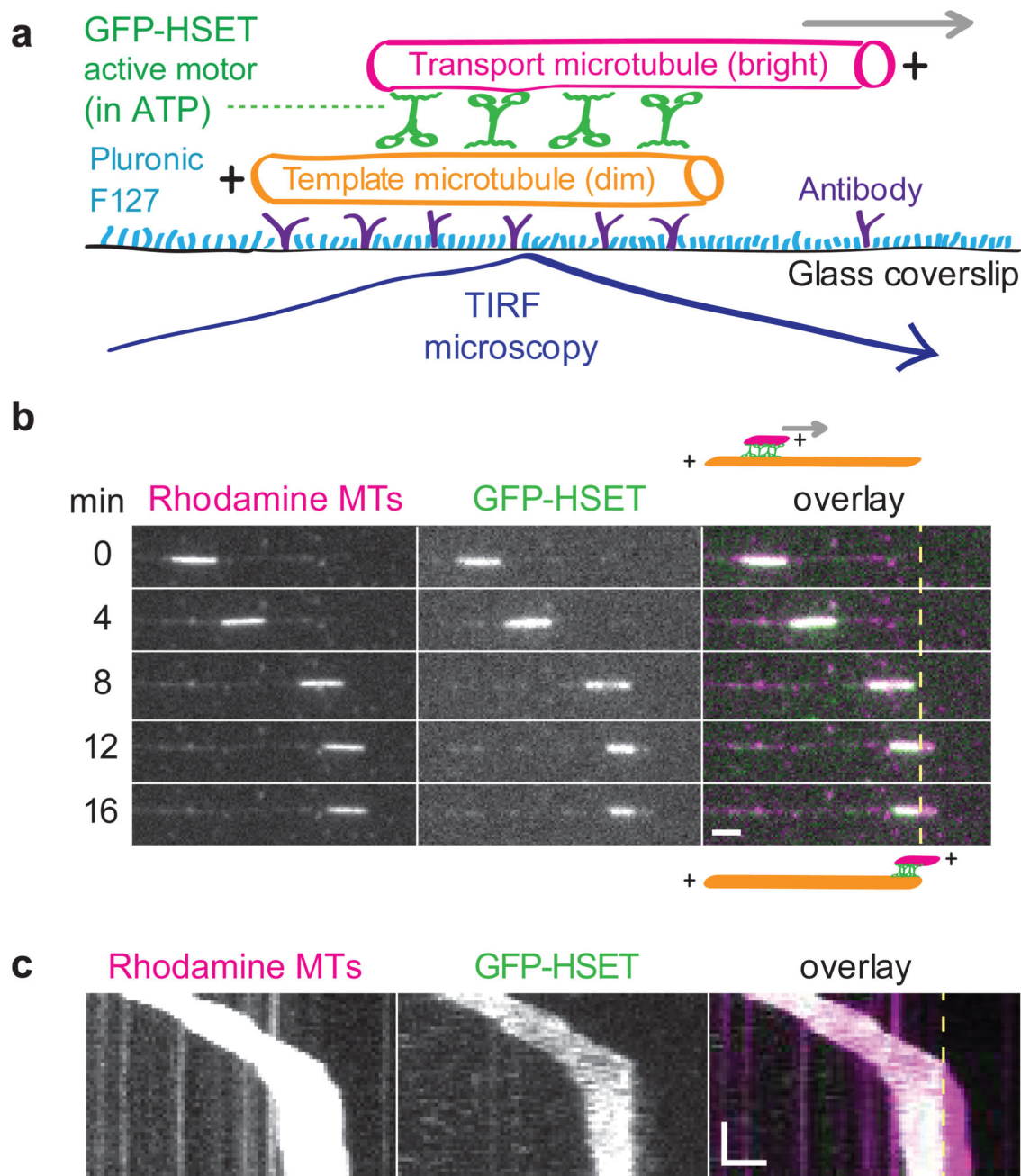
Figure 1. HSET-driven microtubule sliding slows down when microtubules start to slide apart.
(**a**) Schematic representation of GFP-HSET-driven sliding of a transport microtubule (sliding direction indicated by the grey arrow) along a surface-immobilized template microtubule.
(**b**) Time-lapse fluorescence micrographs of a transport microtubule (bright magenta) sliding along a template microtubule (dim magenta) at 1.5 nM GFP-HSET (green) in solution. Fully overlapping microtubules initially slide at constant velocity. Sliding slows down when the microtubules start to slide apart. The dashed line indicates the position of the minus end of the template microtubule. The schematic diagrams indicate the positions of the template

(orange) and the transport (magenta) microtubules at the beginning and at the end of the experiment, respectively. Microtubule plus-ends are indicated. (**c**) Multichannel kymographs representing the time-lapse fluorescence data presented in panel (b). The slope of movement is initially constant, indicating a constant sliding velocity, until the transport microtubule reaches the end of the template microtubule, causing a drastic decrease in the sliding velocity. Scale-bars are 2 μm horizontal and 5 min vertical.
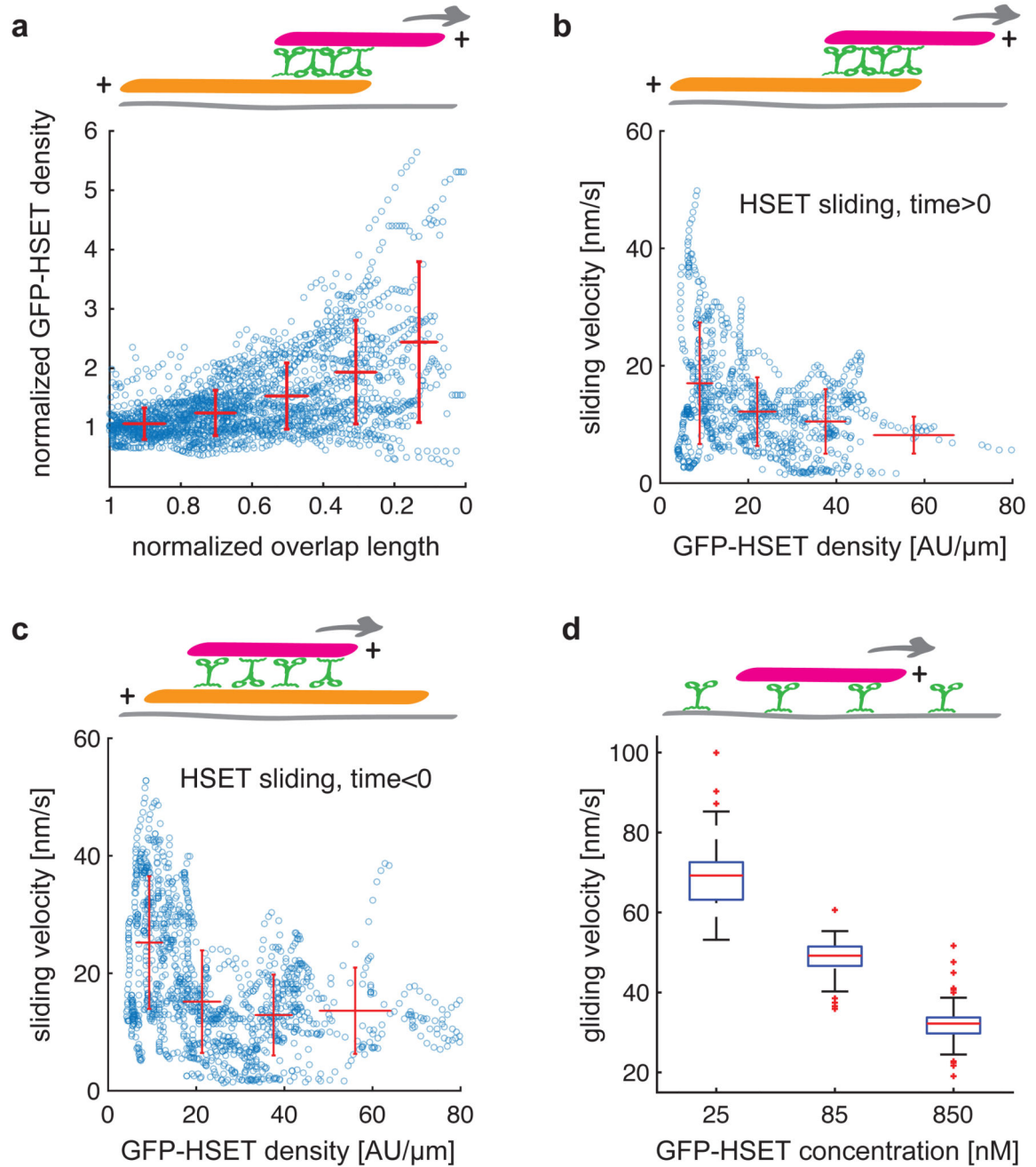
Figure 2. HSET-driven microtubule sliding slows down with increasing motor density.
(**a**) The density of GFP-HSET increases as the microtubule overlap shortens when two microtubules slide apart (events as presented in Fig. 1). GFP-HSET density and overlap length were normalized to unity at the moment when the microtubules started to slide apart. Blue data points indicate combined measurements from 33 sliding events. Red crosses indicate binned and averaged values (± SD). (**b**) The increase in GFP-HSET density (same raw data as in panel **a**) correlates with a decrease in the velocity of microtubule sliding. Blue data points indicate the combined measurements. Red data crosses indicate binned and

averaged values (± SD). Time was set to zero, when the microtubules started to slide apart. (**c**) The increase in GFP-HSET density also correlates with a decrease in the velocity for fully overlapping microtubules. Blue data points indicate combined measurements from 67 sliding events. Red data crosses indicate binned and averaged values (± SD). (**d**) The gliding velocity of microtubules driven by surface-immobilized HSET molecules decreases upon increasing the HSET concentration in solution used for the surface coating, i.e. with an increasing HSET density on the coverslip surface. For microtubules longer than 1.5 μm, which were analyzed here, the gliding velocity was independent of the microtubule length (Supplementary Fig. 2a). Gliding experiments were performed at three different HSET concentrations, namely 25 nM (n = 88 microtubules), 85 nM (n = 75) and 850 nM (n = 82) and the observed velocities are presented in box and whisker plots.
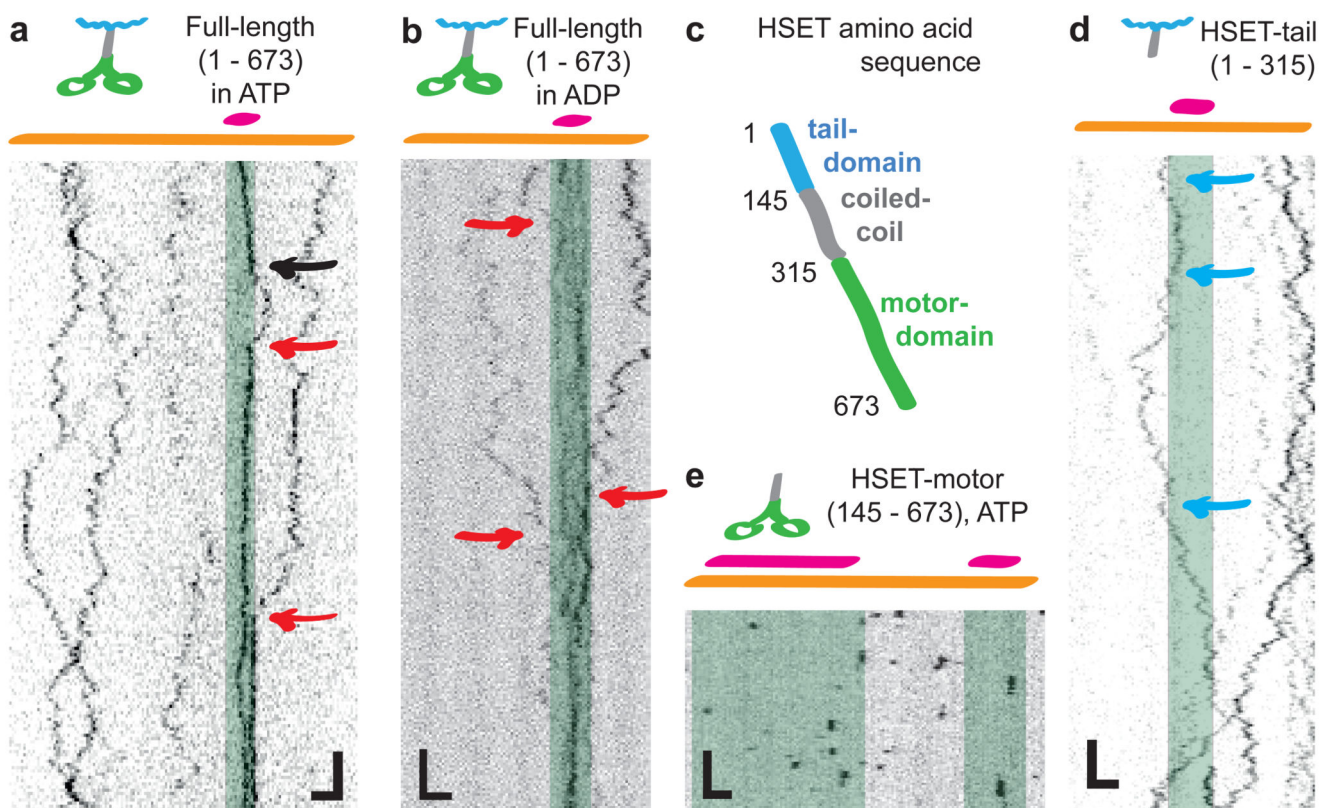
Figure 3. Full-length GFP-HSET diffuses with different diffusion constants on single microtubules and in microtubule overlaps.

(**a**) Kymograph showing single full-length GFP-HSET molecules at a concentration of 0.1 nM diffusing along a single microtubule and in a microtubule overlap in the presence of 1 mM ATP. The position of the microtubule overlap is indicated by the grey transparent box overlaid with the kymograph. Occasionally, single GFP-HSET molecules were observed to enter (red arrows) or leave (black arrow) the overlap. (**b**) Kymograph showing single GFP-HSET molecules at concentration of 0.15 nM diffusing along a single microtubule and in a microtubule overlap in the presence of 1 mM ADP (0 mM ATP). Diffusion did not depend on the nucleotide state of HSET - compare to panel **a**. (**c**) Schematic representation of the HSET amino-acid sequence. (**d**) and (**e**) Kymographs showing the interaction of 0.1 nM GFP-HSET-tail (**d**) and 0.1 nM GFP-HSET-motor (**e**) with single microtubules and microtubule overlaps. Microtubule overlaps were formed using 0.15 nM unlabeled HSET. In contrast to full-length GFP-HSET, GFP-HSET-tail diffused freely across the overlap ends (**d**; events marked by blue arrows) and GFP-HSET-motor interacted only shortly with both, single microtubules and microtubule overlaps (**e**). Scale bars are 2 μm horizontal and 2 s vertical.
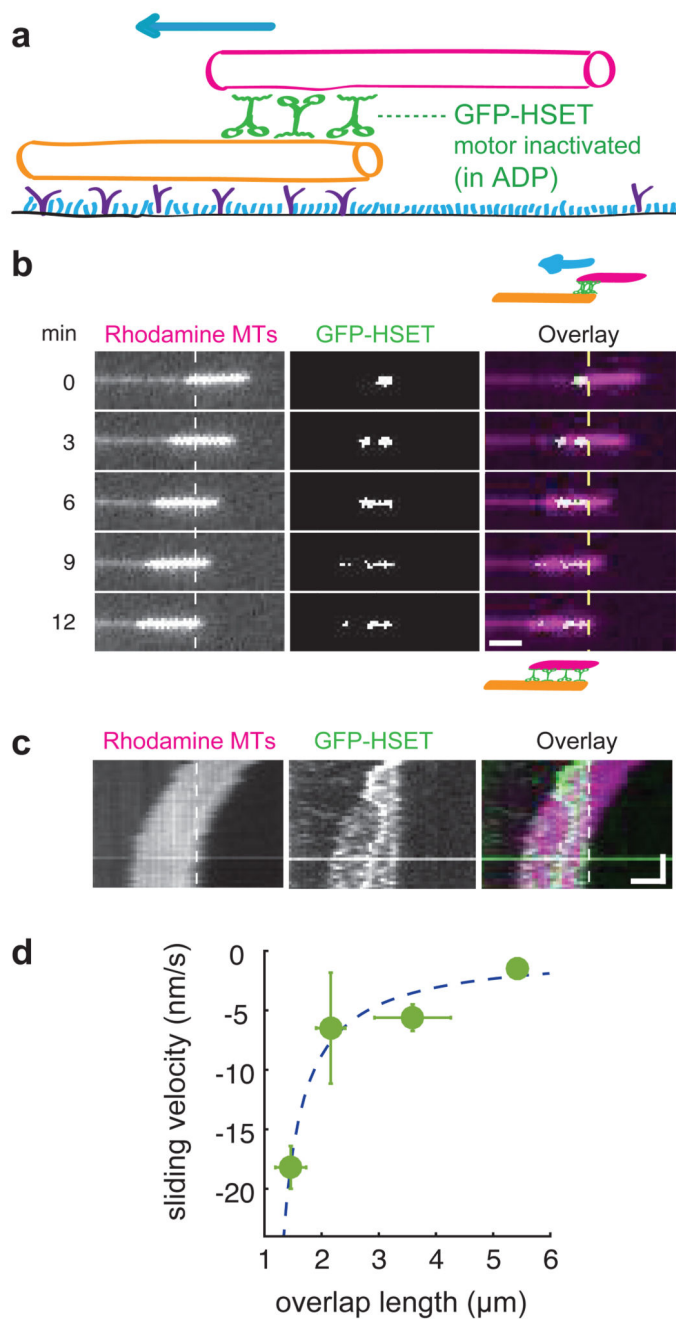
Figure 4. HSET confined in partial microtubule overlaps generates entropic forces.
(**a**) Schematic representation of the experiment with HSET-mediated microtubule sliding in the presence of 1 mM ADP (0 mM ATP). (**b**) Time-lapse fluorescence micrographs of the transport microtubule sliding along a template microtubule (magenta) driven by the presence of ADP-bound GFP-HSET (green) confined in the microtubule overlap. All unbound GFP-HSET was removed from solution before the beginning of imaging. Transport microtubules always moved in the direction of increasing overlap length. The dashed line indicates the position of the minus end of the template microtubule. (**c**) Multichannel kymograph

representing the time-lapse fluorescence data presented in panel **b**. Scale-bars are 3 μm horizontal and 5 min vertical. (**d**) The absolute velocities of overlap expansion (binned and averaged values, mean ± SD) decreased hyperbolically with the lengths of the microtubule overlaps ($n = 8$ microtubule pairs; overlap expansion is expressed using negative values because the microtubules moved in opposite direction compared to motor-driven sliding). The hyperbolic dependence is a signature of entropic forces generated by diffusible crosslinkers confined in the overlap22.
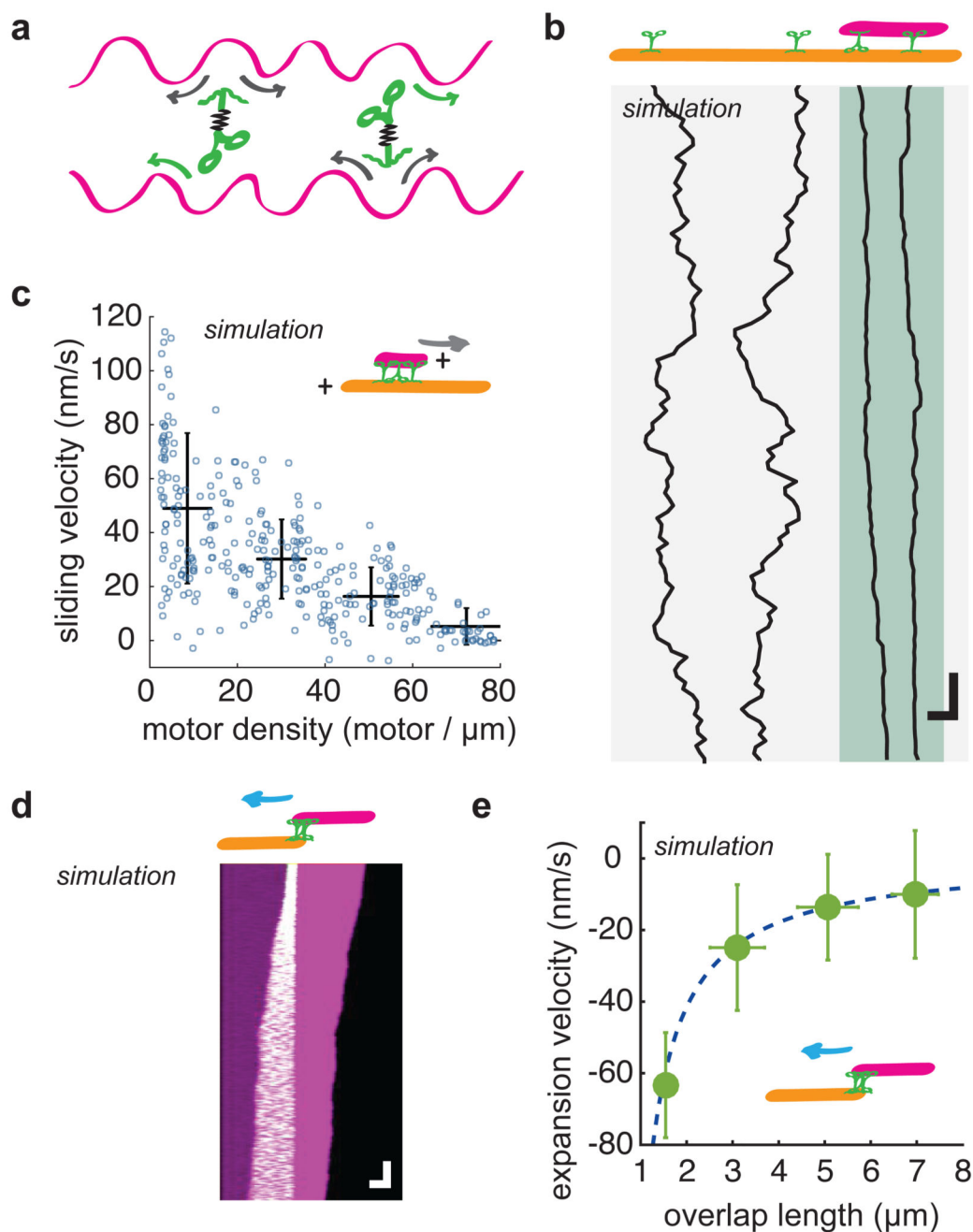
Figure 5. Simulation of diffusible motors confined in a microtubule overlap explains the regulatory feedback by HSET.

(**a**) Microtubules are modeled as one-dimensional array of binding sites. Motors are simulated as harmonic springs, whose ends hop randomly (tail-domain) and directionally (motor-domain) between neighboring binding sites on the microtubules (Methods). (**b**) Kymograph showing the simulated diffusion of individual motors along a single microtubule and in a microtubule overlap. The fast diffusion on the single microtubule is mediated exclusively by the tail-domain. The slow diffusion in the overlap (dark grey area) is

explained by the high binding and unbinding rates of the motor-domain (compare to experimental data in Fig. 3a). The cartoon on top of the kymograph represents the positions of the template (orange) and transport (magenta) microtubules. Scale bars are 2 μm horizontal and 2 s vertical. (**c**) The simulated sliding velocity of fully overlapping microtubules decreases with increasing motor density in the overlap ($n = 22$ simulated events; blue points indicate the simulated data, black crosses indicate the binned and averaged values ($\pm$ SD); compare to experimental data in Fig. 2c). (**d**) Simulated kymograph of microtubule sliding driven by HSET in presence of ADP (compare to experimental data in Fig. 4c). ATP-independent microtubule sliding was simulated using the molecular motors described in **b**, which had their maximum force set to zero (Methods). Scale bars are 1 μm horizontal and 5 s vertical. (**e**) The absolute values of the simulated velocities of overlap expansion (binned and averaged values ($\pm$ SD)) decrease hyperbolically with the lengths of the microtubule overlaps in events as presented in **d** ($n = 9$ simulated events; velocity is expressed using negative values; compare to experimental data in Fig. 4d).
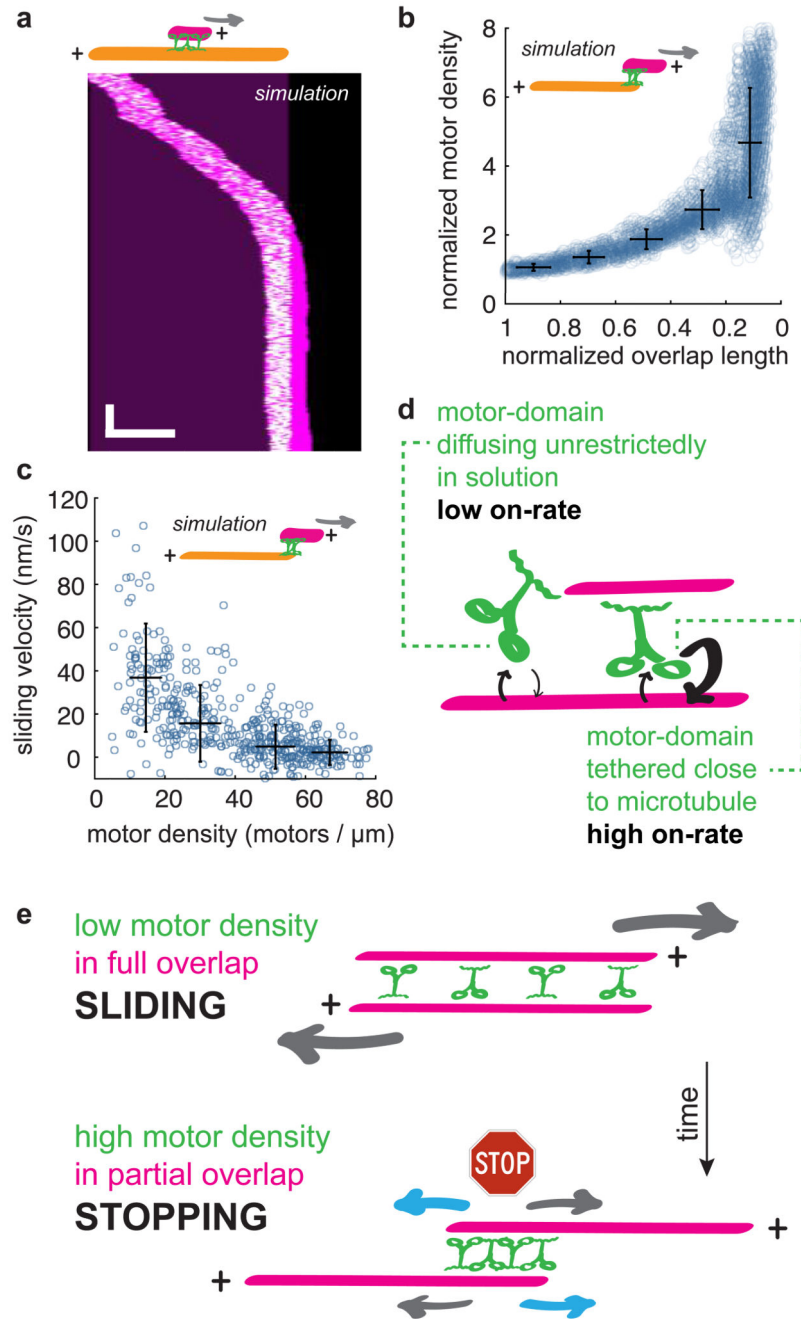
Figure 6. Kinesin-14-driven microtubule sliding is regulated by changes in microtubule overlap length.

(**a**) Kymograph representing a simulated event of HSET-driven sliding of a transport microtubule over the end of a template microtubule. In agreement with our experimental data, we observed that the transport microtubule slowed down as the two microtubules started to slide apart (compare to experimental data in Fig. 1c). Scale bars are 0.5 μm horizontal and 5 s vertical. (**b**) The motor density in the overlap increases as the microtubules start to slide apart in events as presented in **a** (*n* = 15 simulated events; blue points indicate the simulated data, black crosses indicate the binned and averaged values (±

SD)). Motor density and overlap length were normalized to unity at the moment when the microtubules started to slide apart (compare to experimental data in Fig. 2a). (**c**) The increasing motor density in shortening microtubule overlaps in events as shown in **a** correlates with a decreasing sliding velocity (n = 15 simulated events; blue points indicate the simulated data, black crosses indicate the binned and averaged values ($\pm$ SD); compare to experimental data in Fig. 2b). (**d**) Tethering the HSET tail-domain to a microtubule increases the effective net binding rate of the HSET motor-domain to an adjacent microtubule. (**e**) Schematic representation of the regulatory feedback mechanism by HSET: as microtubules start to slide apart, the diffusible HSET molecules are retained within the microtubule overlap, leading to a density-dependent decrease in the sliding velocity (grey arrows) and an increase in an entropic force counteracting the sliding (blue arrows).